Local RNA Conformational Dynamics Revealed by 2-Aminopurine Solvent Accessibility†

Jeff D. Ballin,‡ James P. Prevas,‡ Shashank Bharill,§ Ignacy Gryczynski,|| Zygmunt Gryczynski,§ and Gerald M. Wilson*,‡

Department of Biochemistry and Molecular Biology and Marlene and Stewart Greenebaum Cancer Center, University of Maryland School of Medicine, Baltimore, Maryland 21201, Department of Molecular Biology and Immunology, Health Science Center, University of North Texas, Fort Worth, Texas 76107, and Department of Cell Biology, Health Science Center, University of North Texas, Fort Worth, Texas 76107

Received March 20, 2008

ABSTRACT: Acrylamide quenching is widely used to monitor the solvent exposure of fluorescent probes in vitro. Here, we tested the utility of this technique to discriminate local RNA secondary structures using the fluorescent adenine analogue 2-aminopurine (2-AP). Under native conditions, the solvent accessibilities of most 2-AP-labeled RNA substrates were poorly resolved by classical single-population models; rather, a two-state quencher accessibility algorithm was required to model acrylamide-dependent changes in 2-AP fluorescence in structured RNA contexts. Comparing 2-AP quenching parameters between structured and unstructured RNA substrates permitted the effects of local RNA structure on 2-AP solvent exposure to be distinguished from nearest neighbor effects or environmental influences on intrinsic 2-AP photophysics. Using this strategy, the fractional accessibility of 2-AP for acrylamide (f_a) was found to be highly sensitive to local RNA structure. Base-paired 2-AP exhibited relatively poor accessibility, consistent with extensive shielding by adjacent bases. 2-AP in a single-base bulge was uniformly accessible to solvent, whereas the fractional accessibility of 2-AP in a hexanucleotide loop was indistinguishable from that of an unstructured RNA. However, these studies also provided evidence that the f_a parameter reflects local conformational dynamics in base-paired RNA. Enhanced base pair dynamics at elevated temperatures were accompanied by increased f_a values, while restricting local RNA breathing by adding a C-G base pair clamp or positioning 2-AP within extended RNA duplexes significantly decreased this parameter. Together, these studies show that 2-AP quenching studies can reveal local RNA structural and dynamic features beyond those that can be measured by conventional spectroscopic approaches.

The fluorescent nucleic acid base analogue 2-aminopurine (2-AP)[1] is widely employed in biochemical research. Its red-shifted absorption relative to that of typical nucleic acids and proteins in conjunction with the extreme sensitivity of 2-AP fluorescence to local environmental factors has facilitated its use in structural dynamics studies of nucleic acids alone or in interactions with other biomolecules (*1–5*). Stimulated by the utility of 2-AP in biological research, several studies have characterized 2-AP in well-defined systems, exploring how 2-AP fluorescence is affected by the distance from nucleic acid termini (*6*), stacking dynamics (*7, 8*), and sequence dependence (*9–11*). Neither base pairing nor hydrogen bonding has been found to significantly impact 2-AP fluorescence (*12, 13*). However, all nucleotide bases can quench 2-AP by both static and dynamic mechanisms (*12*). Collisional processes constitute a major pathway in 2-AP quenching: elimination of conformational motion in 2-AP-labeled duplex DNA by cooling to 77 K resulted in 2-AP emission comparable to that of free 2-AP (*8*).

Our previous study used 2-AP fluorescence to monitor helix−coil transitions from various positions within a structurally unambiguous RNA hairpin (*4*). Thermodynamic parameters were thus obtained from diverse perspectives within the model RNA substrate, which in turn revealed features of local RNA conformational dynamics. However, modulation of fluorophore quantum yield is only one indicator of change in the local chemical environment. More sophisticated approaches include changes in dynamic fluorescence quenching. Collisional quenchers such as iodide anion, cesium salts, and acrylamide are often used to assess the solvent accessibility of a fluorophore (*14*). Specific applications of this technique have been used to study protein−protein interactions (*15–17*), protein−ligand associa-

† This work was supported by NIH/NCI Grant CA102428 and a competitive supplement from the Division of Cancer Biology (NIH/NCI) under the Activities to Promote Research Collaborations initiative (to G.M.W.). Additional support was provided by U.S. Public Health Service Grant P20 MD001633 (to S.B.) and the Office of the Dean, University of Maryland School of Medicine (to J.P.P.).

* To whom correspondence should be addressed: Department of Biochemistry and Molecular Biology, University of Maryland School of Medicine, 108 N. Greene St., Baltimore, MD 21201. Telephone: (410) 706-8904. Fax: (410) 706-8297. E-mail: gwils001@umaryland.edu.

‡ University of Maryland School of Medicine.

§ Department of Molecular Biology and Immunology, Health Science Center, University of North Texas.

|| Department of Cell Biology, Health Science Center, University of North Texas.

[1] Abbreviations: 2-AP, 2-aminopurine; SASA, solvent accessible surface area.

10.1021/bi800487c CCC: $40.75
Published on Web 06/11/2008

tion (*18, 19*), membrane−protein biophysics (*16, 20*), protein conformational changes (*21, 22*), and protein−nucleic acid interactions from the perspective of the protein (*23–26*). Fluorescence quenching studies using 2-AP as the probe have been used to monitor DNA structural dynamics (*27, 28*) and protein−DNA interactions from the perspective of the DNA (*29, 30*). Collisional quenching of 2-AP has also been used in a few RNA-based systems to track RNA conformational changes (*31, 32*), drug binding to rRNA (*33*), and protein−RNA association (*34*). Typically, these quenching studies measure variations in the fluorescence of 2-AP-labeled nucleic acid substrates across titrations of a collisional quencher, detecting local conformational changes based on the premise that occlusion of solvent exposure will decrease the sensitivity of 2-AP fluorescence to the quencher. However, broader applications of this strategy are currently hampered by several limitations in our understanding of 2-AP solvent accessibility in nucleic acid contexts. For example, it is unclear how 2-AP solvent exposure varies between specific nucleic acid secondary structural motifs. This information could provide a diagnostic for spectroscopically determining local secondary structure or more accurately describing conformational changes as a consequence of some stimulus. In addition, data from some published studies employing acrylamide titrations to evaluate 2-AP solvent accessibility in DNA or RNA contexts show significant downward curvature on classical Stern−Volmer plots (*27, 33*), suggesting the presence of multiple quenching mechanisms or conformational subpopulations.

In this study, we have addressed these questions by evaluating the solvent accessibility of 2-AP using acrylamide fluorescence quenching in three archetypal RNA structural contexts. Using a previously described family of RNA hairpin substrates (*4*), 2-AP residues were unambiguously positioned within the base-paired stem, in the loop cap, and as a single unpaired base. The sensitivity of 2-AP fluorescence to acrylamide was measured in each of these model RNA hairpins and corresponding unstructured RNA control substrates to distinguish primary versus secondary RNA structural effects on 2-AP solvent exposure. These data resolved unique solvent accessibility characteristics for each 2-AP-labeled position and demonstrated the utility of bimodal algorithms for analysis of 2-AP quenching in structured RNA environments. However, these studies also suggested that acrylamide quenching of 2-AP was highly sensitive to the dynamics of base pair formation in structured RNA. This hypothesis was then tested under conditions where RNA breathing dynamics were altered by varying temperature, adding distal base-paired clamps to the RNA substrate, and positioning 2-AP in extended duplex RNAs. Together, these studies show that acrylamide quenching of 2-AP can monitor localized base pair dynamics in structured RNA molecules, to a degree not readily apparent with other spectroscopic methods.

EXPERIMENTAL PROCEDURES

Reagents. For all experiments, solutions were buffered with potassium HEPES (Sigma) titrated to pH 7.4 using concentrated acetic acid (American Bioanalytical). Potassium acetate and magnesium acetate (Mallinckrodt) served as additional sources of monovalent and divalent cations,

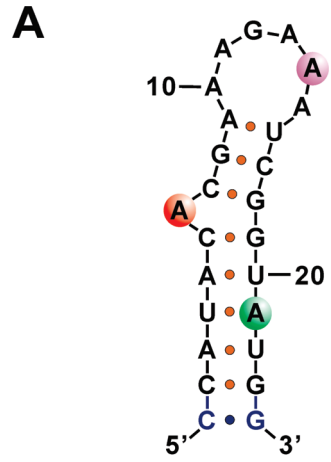

B

```
HP6    5′- CAUACACGAAAGAAAUCGGUAUG -3′
HP14   5′- CAUACACGAAAGAAAUCGGUAUG -3′
HP21   5′- CAUACACGAAAGAAAUCGGUAUG -3′
HP21s  5′-CCAUACACGAAAGAAAUCGGUAUGG-3′
C6     5′- CAUACACG                -3′
C14    5′-         AAAGAAAU        -3′
C21    5′-                 UCGGUAUG -3′

cHP    3′- GUAUGUGCUUUCUUUAGCCAUAC -5′
```

FIGURE 1: 2-AP-labeled RNA substrates. (A) Validated structure of RNA hairpin substrates as previously described (*4*). Spheres denote the sites of specific 2-AP substitutions for each sequence (position 6 in red, position 14 in purple, and position 21 in green). The blue C-G base pair at the base of the RNA hairpin indicates the additional sequence elements present in HP21s. (B) Nomenclature and sequence alignment of the RNA substrates, highlighting the 2-AP position using the same color scheme used in panel A.

respectively. Urea and acrylamide (American Bioanalytical) were Ultra Pure grade (>99.9%).

Model RNA Substrates. All 2-AP-labeled RNA substrates were synthesized, 2′-hydroxyl deprotected, and purified by Dharmacon Research. The unlabeled complementary RNA substrate (cHP) was synthesized and purified by Integrated DNA Technologies. All oligonucleotides were resuspended in ultrapurified water and quantified by the A_{260} in a 10 mM potassium HEPES/acetic acid mixture (pH 7.4) containing 9 M urea, using extinction coefficients provided by the manufacturers. The following extinction coefficients (ε_{260}, liters per mole per cm) were used: HP6, 233400; HP14, 237000; HP21, 232200; C6, 68700; C14, 87700; C21, 68600; HP21s, 249300; and cHP, 225700. 2-AP-labeled RNA hairpins denoted HP*XX* were based on the sequence 5′-CAUACACGAAAGAAAUCGGUAUG-3′, where the internal number (*XX*) indicates the position of the single A → 2-AP substitution within each RNA substrate. Previously (*4*), we demonstrated that each of these RNA substrates forms a hairpinlike fold incorporating an 8 bp stem with a single unpaired base in the 6 position and capped with a six-base loop (Figure 1A). 2-AP labeling sites were chosen as being representative of secondary structural environments commonly found in structured RNA molecules: at the single unpaired base (HP6), in the loop (HP14), or within the stem (HP21). Many structured RNAs possess individual unpaired bases (*35*), which can be intercalated (*36*) or turned outside the RNA helix (*37, 38*). Local RNA structures containing six-membered loops are seen within the HIV-1 transactivation response (TAR) element (*39, 40*) and the internal

ribosome entry site of poliovirus (*41*). These loops demonstrate significant local conformational heterogeneity and are required for recognition and binding by trans-acting factors. The oligonucleotide HP21s includes an additional G-C pair at the terminus of the stem domain (Figure 1), while the sequence of cHP is complementary to those of the 23 bp 2-AP-labeled RNA hairpins. Eight-base control RNA substrates contained sequences equivalent to portions of the model hairpin with 2-AP at the 6 position and are designated by C*XX*, where *XX* indicates the corresponding 2-AP labeling position in the full-length hairpin sequence (Figure 1B). Parallel experiments were performed on free 2-AP and the C*XX* control substrates to permit intrinsic photophysical and/or nearest neighbor effects on 2-AP fluorescence to be distinguished from the consequences of local RNA secondary structure. Previous computational modeling and thermal denaturation experiments showed no evidence of stable structure for any of the 8-mer control RNA substrates (*4*). The purity and structural integrity of all hairpin sequences were verified by denaturing polyacrylamide gel electrophoresis with SYBR Gold stain (Invitrogen). No evidence of RNA degradation was observed, even under overloaded conditions (data not shown).

To generate double-stranded cHP−HP*XX* RNA duplexes, 2-AP-labeled hairpin RNA substrates HP6, HP14, and HP21 (1.2 μM) were mixed with a 3-fold molar excess of cHP in 50 mM KOAc, 5 mM $Mg(OAc)_2$, and 10 mM KHEPES/HOAc in a final volume of 100 μL. Samples were heated to 85 °C for 5 min and then cooled with a linear temperature gradient to 20 °C over a 30 min interval using a Bio-Rad iCycler PCR machine. Quantitative hybridization of HP*XX* oligoribonucleotides was verified in parallel annealing reactions containing ^{32}P trace-labeled hairpin RNA substrates, prepared using [γ-^{32}P]ATP (New England Nuclear) and T4 polynucleotide kinase (Promega) as described previously (*42*). Aliquots of radiolabeled RNAs (each as a double-stranded duplex and as a single-stranded hairpin) were fractionated by electrophoresis through a 12% native polyacrylamide gel in 1× TBE buffer. Visualization of dried gels by Phosphorimager analysis (GE Biosciences) revealed no detectable ^{32}P-labeled single-stranded products following the annealing process (data not shown).

Steady-State Fluorescence Measurements. All steady-state fluorescence experiments were performed using 1 cm × 1 cm quartz cuvettes in a Cary Eclipse fluorometer (Varian). Five nanometer excitation and emission slits were used for all experiments involving single-stranded control and hairpin RNA substrates unless otherwise specified. Fluorescence experiments with double-stranded HP*XX*−cHP duplexes were performed with 5 nm excitation and 10 nm emission slits. Excitation was at 303 nm. In cases where a single wavelength is monitored (e.g., acrylamide quenching), fluorescence emission was measured at 370 nm. No inner filter corrections were necessary because the maximal absorbance beyond 300 nm was below 0.1 for all solutions. Also, no photobleaching was observed within the experimental time scale.

Thermal Denaturation Studies. The thermodynamic stability of HP21s folding was assessed by thermal denaturation of samples containing 800 nM RNA, 10 mM KHEPES/HOAc (pH 7.4), 50 mM KOAc, and 5 mM $Mg(OAc)_2$. Thermal denaturation studies of HP*XX*−cHP duplexes were performed using 800 nM HP*XX* quantitatively annealed to cHP as described above. Cuvettes were equilibrated at 12 °C for HP21s or 17 °C for the HP*XX*−cHP duplex for 10 min before initiation of a 1 °C/min temperature gradient to 88 °C. 2-AP fluorescence (370 nm) was recorded at 0.5 °C intervals using a Cary Eclipse fluorometer equipped with a Peltier temperature controller and in-cell temperature probe. Apparent melting temperatures (T_m) were determined as the extrema of the derivative of fluorescence with respect to temperature calculated within a ±2 °C window.

Steady-State Acrylamide Quenching Studies. The solvent accessibility of 2-AP residues was monitored by collisional quenching with acrylamide. Titration stocks were made with ~1 M acrylamide, 10 mM KHEPES (pH 7.4), and either 50 mM KOAc with 5 mM $Mg(OAc)_2$ or 9 M urea for native or denaturing solutions, respectively. The titration stock was added and manually mixed via pipetting before the fluorescence emission at 370 nm was read. The RNA concentration was typically 400 nM, with the following exceptions to compensate for differences in quantum yield: 2-AP, 200 nM; HP21 and HP21s, 800 nM; HP*XX*−cHP duplex, 1.2 μM. The temperature was controlled via a Peltier temperature controller and in-cell temperature probe. Nonlinear regression analysis of data was performed using Prism version 3.03 (GraphPad), fitting to variations of the standard Stern−Volmer equation (*14*):

$$\frac{F_0}{F_i} = 1 + K_{SV}[Q] \quad (1)$$

where F_0 is the steady-state fluorescence in the absence of acrylamide, F_i is the fluorescence of the sample in the presence of acrylamide at concentration [Q], and K_{SV} is the Stern−Volmer constant describing the average sensitivity of the fluorophore to acrylamide for the single-population analysis in eq 1. A modified form of the Stern−Volmer equation (*14*) assumes that only a fraction of the fluorophore population (f_a) is accessible to acrylamide:

$$\frac{F_0}{F_i} = \frac{1 + K_a[Q]}{1 + (1 - f_a)K_a[Q]} \quad (2)$$

where K_a is the sensitivity of that fraction to acrylamide quenching. The two-state analysis in eq 2 assumes that the inaccessible fluorophore fraction ($1 - f_a$) is completely protected from the quenching compound. While eq 2 is a two-state model in the thermodynamic sense, it does not preclude the existence of additional conformational states with a distribution of relative accessibilities and quenching sensitivities. However, this two-state delineation can serve as a useful parametrization to distinguish differences in fluorophore solvent accessibility in systems presenting significant conformational heterogeneity. Note that eq 2 simplifies to eq 1 when $f_a = 100\%$. Not surprisingly, when the 95% confidence interval of f_a includes $f_a = 100\%$, eq 1 also adequately fits the data [e.g., C21 under native conditions (Table 1)]. When the K_a parameters were very large (e.g., free 2-AP), the f_a resolved to greater than 100%. These cases were alternatively fit to a quenching sphere of action model (*14*):

$$\frac{F_0}{F_i} = (1 + K_{SV}[Q])e^{V[Q]} \quad (3)$$

Table 1: Acrylamide Quenching Parameters for RNA Substrates Determined at 25 °C

	50 mM KOAc, 5 mM $Mg(OAc)_2$					9 M urea				
RNA substrate	f_a (%)[a]	K_a (M^{-1})[a]	V (M^{-1})[b]	K_{SV} (M^{-1})[b]	n	f_a (%)[a]	K_a (M^{-1})[a]	V (M^{-1})[b]	K_{SV} (M^{-1})[b]	n
HP6	103.3 ± 0.9	17.17 ± 0.42	0.62 ± 0.17[c]	17.10 ± 0.45[c]	6	89.4 ± 6.4	4.73 ± 0.54		3.98 ± 0.06[d]	8
C6	82.3 ± 3.3	10.65 ± 0.95		7.22 ± 0.14[d]	6	84.4 ± 5.4	4.86 ± 0.50		3.73 ± 0.04[d]	6
HP14	64.4 ± 1.8	9.72 ± 0.56			5	84.9 ± 3.2	4.26 ± 0.25		3.34 ± 0.02[d]	7
C14	65.3 ± 3.4	8.28 ± 0.86			3	88.6 ± 3.9	5.36 ± 0.39		4.40 ± 0.05[d]	4
HP21	57.2 ± 2.1	9.84 ± 0.83			8	89.6 ± 5.5	4.24 ± 0.40		3.60 ± 0.04[d]	10
C21	87.4 ± 2.5	10.61 ± 0.67		8.09 ± 0.13[d]	3	87.9 ± 7.3	4.59 ± 0.60		3.78 ± 0.06[d]	5
HP21s	28.3 ± 2.5	9.6 ± 1.8			7	90.7 ± 9.3	3.67 ± 0.60		3.11 ± 0.04[d]	7
2-AP	101.5 ± 0.2	37.65 ± 0.37	0.62 ± 0.10[c]	37.58 ± 0.39[c]	4	102.5 ± 2.2	17.8 ± 1.0	0.46 ± 0.41[c]	17.7 ± 1.1[c]	3
HP14-cHP[e]	32.5 ± 1.5	13.0 ± 1.4			3	n/d[f]	n/d[f]	n/d[f]	n/d[f]	
HP21-cHP[e]	44.3 ± 2.8	7.31 ± 0.86			4	n/d[f]	n/d[f]	n/d[f]	n/d[f]	

[a] Determined as the average of n replicate experiments analyzed via global nonlinear least-squares analysis to a two-state quenching model (eq 2). The reported errors are the standard deviations of the global fit. Denoted solution conditions also include 10 mM KHEPES (pH 7.4), as described in Experimental Procedures. [b] Parameters resolved by global nonlinear least-squares analysis to the Stern−Volmer equation with ([c]) or without ([d]) consideration of the sphere of action (eq 3 or eq 1, respectively), depending on whether a large apparent K_a value is exhibited. The reported errors are the standard deviation of the global fit. Values are not included for RNA substrates where regression of 2-AP fluorescence versus [acrylamide] data sets using single-population models was deemed inappropriate by residual runs tests ($P < 0.05$). [c] With consideration of the sphere of action (eq 3). [d] Without consideration of the sphere of action (eq 1). [e] HP*XX*−cHP double-stranded duplex RNA substrates were annealed as described in Experimental Procedures prior to acrylamide titration. [f] Not determined.

which assumes that the fluorophore is immediately quenched after excitation by acrylamide within a sphere with a volume V (reported in units of M^{-1} for convenience). In all cases for which extreme quenching sensitivity was observed, models 2 and 3 fit equivalently in terms of the residual absolute sums of squares. Note that fitting with the additional f_a parameter in cases where the simpler classical Stern−Volmer equation (eq 1) applies results in an increased variance for both fit estimators (f_a and K_a). However, overdetermination does not significantly perturb the mean estimation of the fitted parameters (*43*). Also of note is the fact that data were fitted as F_i/F_0 to the reciprocal of eq 2 because we found that nonlinear regression confidence intervals were improved, although the values of resolved parameters were not significantly affected. However, all data are presented as F_0/F_i versus [acrylamide] to facilitate comparison to classical Stern−Volmer analyses. Since the goal in this study was to estimate differences in structure by comparison of quench constant values, quenching phenomena of 2-AP-labeled species were analyzed using eq 2 for the sake of consistency and ease of interpretation, unless otherwise indicated.

RESULTS

Multistate Algorithms Are Required To Model Acrylamide Quenching of 2-AP in Most RNA Contexts. Acrylamide quenching is a well-established approach to quantify the sensitivity of a fluorophore to a collisional fluorescence quencher (*14*). This sensitivity is in turn a measure of the average solvent exposure of the probe. Here, we used this technique to monitor the solvent exposure of 2-AP in each of several archetypal RNA structural motifs. Using eq 1 to analyze the change in 2-AP fluorescence as a function of acrylamide concentration infers that all 2-AP bases experience similar solvent access across the RNA sample population. While the acrylamide sensitivity of 2-AP fluorescence from some labeled positions was reasonably well described by this model (e.g., Figure 2A, C21), nonlinearity on classical Stern−Volmer plots indicates that this model fails generally for 2-AP in native RNA contexts (e.g., Figure 2A, HP14, C14, and HP21). However, the deviations from idealized linear Stern−Volmer behavior observed in all data sets were accommodated by eq 2, where only a fraction of the 2-AP population (f_a) is considered to be accessible to solvent, with average acrylamide sensitivity K_a. The extent that f_a falls below 100% is reflected in the degree of downward curvature in F_0/F_i versus quencher concentration plots. Thus, 2-AP positioned in the stem position of the native hairpin (HP21) would be considered less solvent exposed than in the native single-stranded C21 (Figure 2A and Table 1). However, when 2-AP is highly solvent exposed, modest upward curvature on the Stern−Volmer plot yields a resolved f_a value slightly but significantly greater than 100%. Here, this was observed for 2-AP in the single unpaired base position (native HP6) and as a free base in solution (Figure 2A and Table 1). Significantly higher K_a values resolved for free 2-AP and native HP6 are reflected by steeper initial slopes in Stern−Volmer plots and indicate that the extent of quenching efficiency is very high. In cases where fluorophores exhibit extreme sensitivity to quenching compounds, upward curvature of Stern−Volmer plots has been interpreted using the sphere of action model described by eq 3, where collisions between quencher and fluorophore immediately following excitation cause the quencher−fluorophore pair to appear as a dark complex (*14*). In this study, all quenching experiments yielding an f_a of >100% by the bimodal quenching model were well resolved by this sphere of action algorithm (Table 1).

Fractional Accessibility to Acrylamide Varies as a Function of 2-AP Placement within Defined RNA Structural Contexts. A key objective of this study was to determine whether parameters describing the sensitivity of 2-AP fluorescence to a collisional quencher correlated with fluorophore presentation in defined local RNA structural motifs. Quencher titrations are frequently used to assess changes in fluorophore solvent exposure resulting from conformational changes or interactions with other factors. However, comparing the acrylamide sensitivity of 2-AP fluorescence from RNA substrates HP6, HP14, and HP21 (Figure 2A) indicates that 2-AP solvent accessibility varies widely as a function of labeling position for otherwise identical RNA hairpin substrates.

Bimodal quenching analyses of hairpin substrates and their corresponding controls were quantitatively compared using

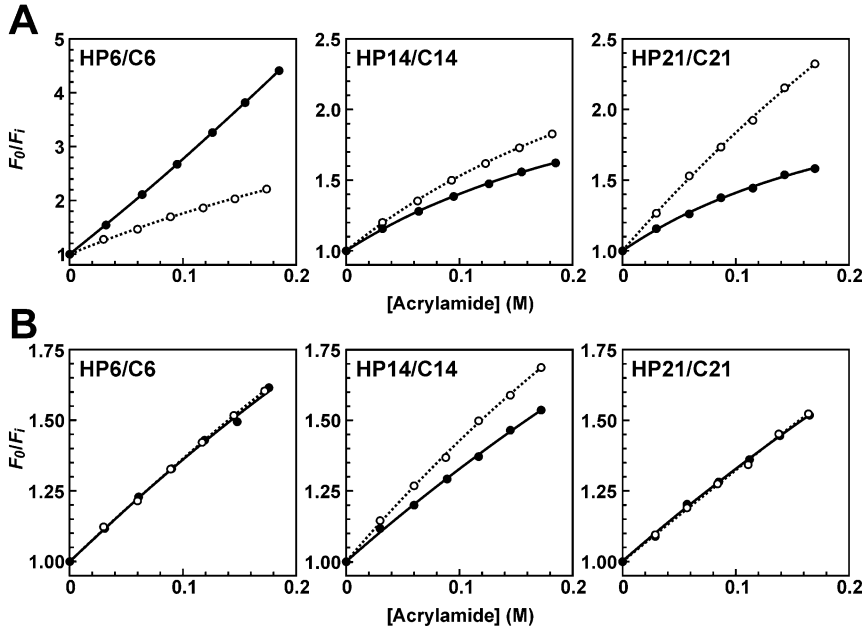

FIGURE 2: Acrylamide quenching titrations of hairpin and control RNA substrates under native and denaturing conditions. Hairpin (●) and control (○) RNA substrates were titrated with acrylamide under (A) native conditions [10 mM KHEPES (pH 7.4) containing 50 mM KOAc and 5 mM $Mg(OAc)_2$] or (B) denaturing conditions [10 mM KHEPES (pH 7.4) containing 9 M urea] at 25 °C, monitoring relative fluorescence loss with respect to increasing acrylamide concentration. Regression solutions (lines) represent nonlinear fits to individual data sets using the bimodal quenching model given by eq 2. Solvent accessibility parameters for each RNA substrate were derived using global regression solutions across multiple data sets and are listed in Table 1.

Table 2: *P* Values from Unpaired Two-Tailed *t*-Test Comparisons of f_a and K_a across RNA Substrates and Solution Conditions

	native conditions[a]		denaturing conditions[a]	
comparison	f_a	K_a	f_a	K_a
HP6 vs C6	*<0.0001*	*<0.0001*	0.149	0.654
HP14 vs C14	0.6332	*0.0266*	0.121	*0.007*
HP21 vs C21	*<0.0001*	0.2739	0.620	0.198
HP6 vs HP14	*<0.0001*	*<0.0001*	0.117	0.055
HP6 vs HP21	*<0.0001*	*<0.0001*	0.944	*0.042*
HP14 vs HP21	*<0.0001*	0.3053	0.061	0.909
C6 vs C14	*0.0002*	*0.0085*	0.220	0.132
C6 vs C21	0.0524	0.9505	0.384	0.436
C14 vs C21	*0.0008*	*0.0208*	0.869	0.063

[a] Native conditions are defined as 50 mM KOAc, 5 mM $Mg(OAc)_2$, and 10 mM KHEPES (pH 7.4). Denaturing conditions are defined as 9 M urea and 10 mM KHEPES (pH 7.4). The parameters f_a and K_a are as defined in eq 2. *P* values denote the level of confidence that a given parameter is indistinguishable between the RNA substrates under comparison. Parameters exhibiting statistically different values between compared RNA substrate pairs are italicized ($P < 0.05$).

unpaired two-tailed *t*-tests, with differences exhibiting $P < 0.05$ considered significant (Table 2). By contrasting the solvent accessibility parameters of 2-AP in each hairpin label position relative to its cognate control RNA, we could distinguish alterations in quenching sensitivity resulting from RNA structural context from the effects of nearest neighbors and/or intrinsic 2-AP photophysics. Previously, we used a similar approach to define the influence of local RNA structural presentation on the quantum yield and fluorescence lifetime properties of 2-AP (*4*). Comparing the acrylamide sensitivity of 2-AP fluorescence from substrates HP6 versus C6 presents the most striking contrast, with HP6 returning a 25% increase in f_a and a 61% increase in K_a (Table 1). This dramatic enhancement of quencher sensitivity is consistent with an extrahelical 2-AP conformation at the hairpin 6 position (Figure 1A). By contrast, quenching analyses of HP14 and C14 yielded fairly similar f_a and K_a values, suggesting that the solvent exposure of 2-AP within the hairpin hexaloop is comparable to that of the fluorophore contained within C14. A distinct case was observed for 2-AP in the base-paired hairpin stem, where the f_a for HP21 was 34% lower than the f_a from the unstructured C21 substrate. However, resolved K_a values could not be distinguished between HP21 and C21. Not surprisingly, free 2-AP shows ~100% accessibility with a K_a value more than double that of HP6. Together, these data indicate that the resolved K_a values for 2-AP vary only slightly as a function of RNA structural presentation, with the exception of constrained, highly solvent exposed contexts such as that anticipated for a single bulged nucleotide (e.g., HP6). However, the fractional accessibility of 2-AP to acrylamide is highly sensitive to RNA structure, with f_a significantly increased in bulged contexts and decreased for paired bases, relative to unstructured control RNAs.

The identity of adjacent residues also modestly influenced 2-AP quenching properties, which is evidenced by comparing solvent accessibility parameters for the control RNA substrates. Under native conditions [50 mM KOAc/5 mM $Mg(OAc)_2$], K_a values for C6 and C21 are statistically indistinguishable but modestly greater than $^{C14}K_a$ (Tables 1 and 2). Fractional accessibilities show a more dramatic trend: $^{C14}f_a < {}^{C6}f_a \approx {}^{C21}f_a$. The rank order in f_a, and to some extent K_a, coincides with the solvent accessible surface area (SASA) of the flanking bases, suggesting that the size of neighboring bases may impact the ability of acrylamide to quench 2-AP fluorescence. Adenine, which flanks 2-AP in C14, cytosine, which flanks 2-AP in C6, and uracil, adjacent to 2-AP in C21, have SASAs of 278, 244, and 235 Å^2, respectively (*44*). This ordering of quenching parameters disappears in 9 M urea, indicating that essentially all base stacking interactions affecting collisional surface area are eliminated under denaturing conditions.

The presence of 9 M urea is expected to fully denature RNA structure and thus abrogate secondary structural effects on quenching phenomena. Under these conditions, f_a and K_a values for C6, C14, and C21 were statistically indistinguishable (Table 2). Also, the striking differences in f_a and/or K_a values observed between HP6 versus C6 and HP21 versus C21 under native conditions are absent at 9 M urea (Table 1). While HP14 and C14 retain similar f_a values under denaturing conditions, K_a is modestly (25%) elevated in C14 versus HP14. The general lack of statistically significant differences between f_a (and to a large extent K_a) values for 2-AP across all denatured RNA contexts suggests that the diversity of quenching parameters observed under native conditions depends on the presence of secondary structure. In 9 M urea, acrylamide quenching of 2-AP in all RNA substrates could also be resolved by the classical Stern−Volmer equation (eq 1), indicating that the solvent exposure of 2-AP can be modeled as a single population within denatured RNA contexts (Table 1).

Finally, comparing the quenching parameters of 2-AP in control RNA substrates under native versus denaturing conditions illustrates the importance of unstructured RNA controls. C6 and C21 show no statistically significant variation in f_a with transfer into 9 M urea ($P = 0.435$ and $P = 0.915$, respectively), indicating that they are effective models of the denatured state. However, ${}^{C14}f_a$ is increased ($P = 0.0004$) in the presence of urea, suggesting that C14 exhibits a partially ordered conformation under native conditions which may involve some degree of stacking between 2-AP and its two adjacent adenines. The tendency of adjacent adenines to stack has been known for at least 40 years (*45, 46*) and has been resolved by NMR (*47*). High concentrations of urea most likely disrupt this ordered stacking, reflected in increased 2-AP solvent accessibility. As such, native C14 is a better representation of the unfolded state of HP14 under native solution conditions than HP14 at 9 M urea where this nearest neighbor effect is absent.

Fractional Solvent Accessibility of 2-AP Reflects Local Conformational Dynamics within Base-Paired RNA. Several observations support the hypothesis that breathing dynamics occur near the termini of the model RNA hairpins. First, limited digestion of folded hairpin substrates with the single strand-specific endonuclease RNase T_2 generated cleavage sites up to three bases from the base of the stem (*4*). Since RNase T_2 exhibited very poor catalytic efficiency within the remaining double-stranded domain of the hairpin RNA (*4*), the stem terminus must be unpaired sufficiently to allow RNA strand cleavage within the time scale of enzyme kinetics. Second, this study indicated significant fractional exposure of the stem-positioned 2-AP to acrylamide (${}^{HP21}f_a = 56\%$), which was surprising given that the fluorophore is positioned three base pairs into the stem. Finally, we observed no evidence of a denatured subpopulation of hairpins by native gel analysis (data not shown), via limited nuclease digestion (*4*), or in the quencher titrations which found that the 6 position 2-AP remains ≈100% exposed and does not relax into the unstructured state represented by C6 (Figure 2A). Together, these data indicate that the native hairpin substrate is stably folded but exhibits localized base pair dynamics near the base of the stem.

Three sets of experiments were used to assess how local RNA base pair dynamics influence 2-AP solvent accessibility

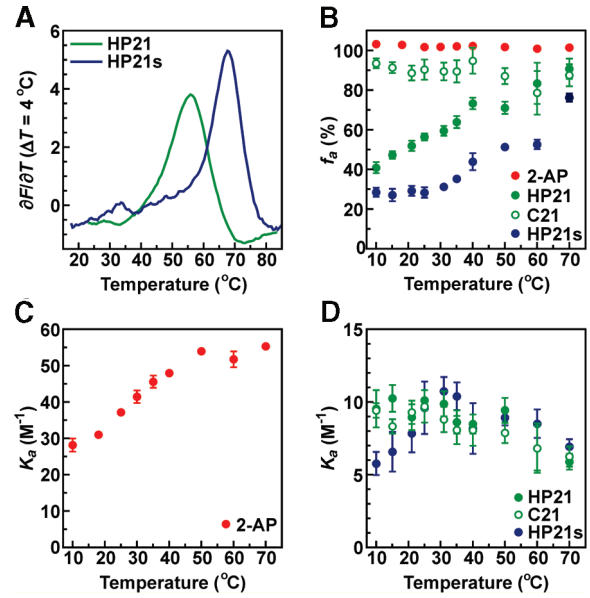

FIGURE 3: Effects of temperature and an additional terminal C-G base pair on the solvent accessibility of 2-AP positioned within the hairpin stem. (A) The derivative of fluorescence emission as a function of temperature was calculated for RNA substrates HP21 and HP21s ($\Delta T = 4$ °C) as described in Experimental Procedures, permitting estimation of transition melting temperatures (T_m) listed in Table 3. (B) The fractional solvent accessibility (f_a) of 2-AP in selected RNA substrates or free in solution was calculated using eq 2 across a series of acrylamide titrations (e.g., Figure 2) performed at various temperatures. The quenching efficiencies of the solvent accessible fraction (K_a) of free 2-AP (C) and selected 2-AP-labeled RNA substrates (D) were determined from acrylamide titration plots using eq 2 as described above and plotted as a function of temperature. In all plots, error bars reflect the standard deviation of each parameter resolved from at least two independent acrylamide titration experiments at each temperature.

parameters. First, acrylamide titrations were performed on HP21 at a variety of temperatures, since localized breathing of double-stranded RNA is enhanced as the temperature increases. Quenching parameters were then compared with analogous studies of C21 and free 2-AP to control for nearest neighbor and intrinsic photophysical effects, respectively. The sensitivity of free 2-AP to quencher was significantly enhanced at higher temperatures, reflected in a 2-fold increase in K_a within a span of 40 °C, reaching a plateau between 50 and 70 °C (Figure 3C). ${}^{HP21}K_a$ and ${}^{C21}K_a$ are nearly indistinguishable across the entire temperature range but show a trend in opposition with ${}^{2\text{-AP}}K_a$ with a weak sensitivity to temperature between 10 and 50 °C and a decreasing magnitude at higher temperatures (Figure 3D). The ratios ${}^{2\text{-AP}}K_a/{}^{HP21}K_a$ and ${}^{C21}K_a/{}^{2\text{-AP}}K_a$ increase from ∼3 to ∼10 as the temperature increases, demonstrating that interactions with nearest neighbors drive the divergence of HP21 and C21 quenching sensitivities from that of free 2-AP. However, the limited variability in K_a for HP21 versus C21 across all tested temperatures indicates little diagnostic utility for this parameter with respect to RNA structure (see Discussion). In contrast, changes in the fractional accessibility of 2-AP within HP21 to acrylamide were consistent with temperature-dependent changes in local RNA duplex breathing. Resolved f_a values for free 2-AP and C21, which exhibit no base pair potential, were relatively constant and near 100% across the 10−70 °C temperature range (Figure 3B). However, ${}^{HP21}f_a$ dramatically increased as a function of temperature, ap-

Table 3: Melting Temperatures and Relative Quantum Yields of 2-AP-Labeled RNA Hairpin Substrates under Native Conditions

RNA substrate	relative quantum yield[a]	T_m (°C)[b]	n[b]
HP14[c]	0.227 ± 0.012	57.3 ± 1.9	6
HP21[c]	0.050 ± 0.002	56.3 ± 1.1	7
HP21s	0.0111 ± 0.0003	67.1 ± 0.4	3
HP14−cHP[d]	0.0107 ± 0.0001	75.9 ± 0.2	2
HP21−cHP[d]	0.0169 ± 0.0009	76.0 ± 0.2	2

[a] Relative quantum yields were determined using 2-AP under identical solution conditions as a ratiometric reference. Each value represents the mean ± the standard deviation for at least three independent samples. [b] Determined as the extremum of the derivative of hairpin RNA substrate fluorescence vs temperature calculated over a ±2 °C window for each 2-AP-labeled position, reported as the mean ± the standard deviation across n independent experiments. [c] Values reported previously (*4*). [d] Melting temperatures and relative quantum yields were determined for hybridized double-stranded RNA composed of the indicated 2-AP-labeled RNA and the unlabeled complementary RNA substrate, cHP (Experimental Procedures).

proaching the level of $^{C21}f_a$ at temperatures beyond the hairpin T_m of 56 °C. The extreme sensitivity of $^{HP21}f_a$ to temperature and its asymptotic approach to $^{C21}f_a$ at temperatures near the hairpin melting point indicate that the fractional solvent accessibility of 2-AP within HP21 is highly sensitive to base pair dynamics near the hairpin terminus.

A second experiment for assessing the relationship between f_a and local duplex breathing employed an extended hairpin sequence, HP21s, which was stabilized by an additional C-G base pair at the stem terminus (Figure 1). We predicted that since the fractional accessibility of 2-AP in HP21 increases as a function of temperature, $^{HP21}f_a$ could be reduced by stabilizing the duplex state. Addition of the C-G base pair to the hairpin stem increased the melting temperature of the hairpin by approximately 11 °C (in Table 3, cf. HP21s vs HP21). Under native conditions at 25 °C, the fractional accessibility of 2-AP in HP21s was 50% lower than in HP21 (Table 1), consistent with enhanced occlusion of the fluorophore from solvent. Across the temperature range of 10−70 °C, $^{HP21s}f_a$ was consistently lower than $^{HP21}f_a$ (Figure 3B), exhibiting behavior expected for a more stably base paired (i.e., buried) probe position: a protracted plateau in quenching accessibility at low and intermediate temperatures, finally increasing in magnitude at higher temperatures and eventually approaching $^{C21}f_a$ at temperatures near T_m.

In a third experiment, the relationship between f_a and local base pair dynamics was tested by localizing 2-AP within extended RNA duplexes. We reasoned that local base pair dynamics would be diminished within an exclusively double-stranded RNA relative to a hairpin of the same sequence, except at the extreme termini, and would further provide an opportunity to quantify 2-AP solvent accessibility at varying positions within an RNA duplex. HP21 and HP14 were quantitatively hybridized to an unlabeled complementary RNA, denoted cHP, as described in Experimental Procedures. Thermal denaturation experiments were used to characterize the thermodynamic stability of the duplexes and to confirm that no significant single-stranded species were detectable. The HP14−cHP and HP21−cHP duplexes each melted in a single sharp transition (Figure 4A), yielding apparent melting temperatures significantly higher than the value of ≈57 °C observed for the corresponding hairpins (Table 3) and consistent with the duplex nature of these substrates. Acrylamide titration experiments then resolved quencher sensitivity

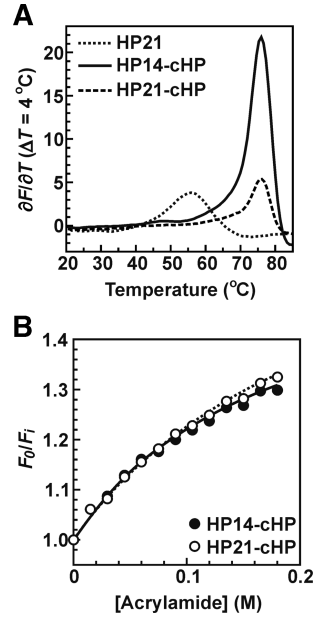

FIGURE 4: Solvent accessibility of 2-AP in extended duplex RNAs. (A) T_m values for the HP14−cHP and HP21−cHP double-stranded RNA duplexes were calculated from the derivatives of fluorescence emission as a function of temperature ($\Delta T = 4$ °C) as described in Experimental Procedures. The derivative melting plot of HP21 is included for comparison. (B) Acrylamide quenching titrations of 2-AP in duplex RNA substrates were performed as described in the legend of Figure 2. Solvent accessibility parameters were resolved by nonlinear regression using eq 2 and are listed in Table 1.

parameters for 2-AP in each of the extended RNA duplex contexts (Figure 4B). Higher concentrations of RNA were required for these experiments because the quantum yield of 2-AP was strongly reduced in the duplexes relative to the hairpins alone (Table 3), typical of 2-AP in highly stacked local environments (*4*). Interestingly, the fractional accessibility of 2-AP in both the HP14−cHP and HP21−cHP duplexes was significantly lower than that observed in the corresponding RNA hairpins under native conditions (Table 1), consistent with diminution of f_a when base pair breathing dynamics are limited.

DISCUSSION

Environmental Factors Can Impact the Sensitivity of 2-AP to Quencher in a Manner Independent of RNA Conformational Events. The two-state quenching model utilizes the parameters f_a and K_a to describe the fractional accessibility of a fluorophore to solvent and its corresponding sensitivity to the quenching compound. This analysis has had extensive use in the protein fluorescence literature but to the best of our knowledge has not been applied to intrinsic fluorophores in nucleic acids. However, while nucleic acid conformational changes are our primary interest, we also noted that quenching parameters could be profoundly affected by factors independent of folding transitions. To this end, we compared the acrylamide sensitivity of free 2-AP across solution environments since 2-AP is fully solvent exposed under both native and denaturing conditions and thus amenable to classical Stern−Volmer analysis in each case.

In the absence of static quenching, the Stern−Volmer quench constant is directly proportional to the product of the unquenched fluorescence lifetime (τ_0), the diffusion-

controlled bimolecular rate constant (k_0), and the quenching efficiency (f_Q) (*14*). The quantity $k_0 f_Q$ is known as the bimolecular quench constant (k_q), thus giving

$$K_{SV} = \tau_0 k_q = \tau_0 f_Q k_0 \quad (4)$$

The diffusion-controlled bimolecular collisional rate constant is described by the Smoluchowski equation

$$k_0 = \frac{4\pi N}{1000}({}_cR_f + {}_cR_q)(D_f + D_q) \quad (5)$$

where N is Avogadro's number, ${}_cR_f$ and ${}_cR_q$ are the collisional radii of the fluorophore and quencher (i.e., acrylamide) respectively, and D_f and D_q are their respective diffusion coefficients (*48*). The diffusion coefficients can be estimated by the Stokes−Einstein equation

$$D = \frac{kT}{6\pi\eta({}_mR)} \quad (6)$$

where k is the Boltzmann constant, T the absolute temperature, η the solvent viscosity, and ${}_mR$ the molecular radius. We first considered the ratio of K_{SV} quench constants with and without urea to define changes in the quenching behavior of free 2-AP (Table 1) that can be ascribed to photophysical effects independent of structural changes. Substituting eqs 5 and 6 into eq 4, taking the ratio of the analogous expressions for native (N) and denaturing (D) conditions at a fixed temperature and rearranging, gives

$$\frac{{}^NK_{SV}}{{}^DK_{SV}} = \frac{{}^N\tau_0\,{}^Nf_Q\,{}^D\eta}{{}^D\tau_0\,{}^Df_Q\,{}^N\eta}\frac{({}^N_cR_f + {}^N_cR_q)({}^N_mR_f + {}^N_mR_q)({}^D_mR_{fm}{}^D_mR_q)}{({}^D_cR_f + {}^D_cR_q)({}^D_mR_f + {}^D_mR_q)({}^N_mR_{fm}{}^N_mR_q)} \quad (7)$$

Intensity-weighted average lifetimes ${}^N\tau_0$ and ${}^D\tau_0$ (10.9 and 10.3 ns, respectively) were resolved in a previous study (*4*). We assumed that the acrylamide quenching efficiency for 2-AP is not affected by the presence of urea on the basis of the fact that acrylamide quenches indole with an f_Q of ≈1 at both 0 and 7.7 M urea (*49*). If the addition of 50 mM KOAc, 5 mM $Mg(OAc)_2$, and 10 mM KHEPES (pH 7.4) has a negligible effect on water viscosity, we can estimate the ratio η^D/η^N from literature data. Quantitative measurements indicate that ~8 M urea exhibits a >66% increase in viscosity relative to pure water (*50*). Extrapolation of the Kawahara and Tanford empirical expression to estimate viscosity at 9 M urea predicts an η^D/η^N of ≈1.8. By this model, consideration of only fluorescence lifetime changes and viscosity effects in eq 7 accounts for more than 90% of the experimentally observed shift in K_{SV} (1.9 calculated from eq 7 versus ${}^NK_{SV}/{}^DK_{SV} = 2.1 \pm 0.1$ for 2-AP). Urea-induced changes in molecular/collisional radii of 2-AP and acrylamide are thus either inconsequential or compensatory under the conditions studied here. These results suggest that the dramatic changes seen for K_{SV} for RNA substrates as a function of denaturant are mostly due to effects of viscosity on diffusion. Interestingly, the RNA control substrates with pyrimidines neighboring the 2-AP label have comparable ${}^NK_a/{}^DK_a$ ratios (C6, 2.2 ± 0.3; C21, 2.3 ± 0.3). Even C14 has a ${}^NK_a/{}^DK_a$ ratio within two standard deviations (1.5 ± 0.2) of that predicted by eq 7, despite known native stacking interactions between adenosines adjacent to the 2-AP which can complicate quenching phenomena (see Results). This cumulatively suggests that, at least when 2-AP is flanked by cytosines or uracils, viscosity accounts for the majority of the change in K_a for unstructured RNA substrates in the absence and presence of urea. These results are consistent with acrylamide quenching studies of the tryptophan derivative NATA which found that differences in K_{SV} could also be primarily attributed to viscosity changes (*49*).

Quenching Sensitivity (K_a) Resolved from the Two-State Quenching Model Is Relatively Insensitive to RNA Secondary Structure. Hairpin versus corresponding control RNA substrates exhibited comparable K_a values under native solution conditions in all cases except the HP6−C6 pair. The observation ${}^{HP6}K_a \gg {}^{C6}K_a$ is not surprising because the 6 position 2-AP moves from a likely extrahelical conformation in HP6 to a partially stacked state within C6. The HP6 bulged position has little possibility of shielding by, or collision with, neighboring bases, whereas these events are highly likely for the 2-AP within the unstructured and single-stranded C6. Note that C6 has K_a values similar to those of other control and hairpin sequences, again suggesting that differences in the adjacent neighbors do not have a strong effect on K_a, unless there are no neighbors at all. Given that K_a is relatively invariant across disparate local structural environments, it appears to have little predictive power when RNA folded states are being evaluated.

Fractional Accessibility to Quencher (f_a) Is Highly Sensitive to RNA Secondary Structure. By comparing parameters derived from acrylamide quenching of 2-AP in RNA hairpins versus corresponding unstructured control RNAs, we noted distinct changes in resolved fractional accessibilities for 2-AP positioned in each secondary structural motif that was tested. For 2-AP in the 6 position of the hairpin substrate (HP6), several observations support assignment of this base as extrahelical, rather than intercalated within the stem. First, ${}^{HP6}f_a$ is equivalent to ${}^{2\text{-}AP}f_a$ at ≈100%, indicating full exposure to the solvent (Table 1). Second, ${}^{HP6}f_a$ is significantly greater than ${}^{C6}f_a$ under native conditions, the sole case in which 2-AP exhibits increased access to the quencher in the folded hairpin relative to its unstructured control RNA. Finally, HP6 presented the only example in which the K_a parameter was informative, since ${}^{HP6}K_a$ was significantly enhanced relative to ${}^{C6}K_a$ and is closer to ${}^{2\text{-}AP}K_a$ than that of any other RNA substrate. By contrast, HP21, HP21s, and the HP21−cHP duplex all exhibited significantly lower f_a values than the C21 control RNA, consistent with extensive shielding of 2-AP through ordered base stacking interactions in the folded or duplex substrates. Conversely, the indistinguishable fluorescence quenching characteristics resolved for HP14 and C14 suggest that 2-AP flanked by adenosines within a hexaloop exhibits dynamics comparable to those within a single-stranded RNA. However, in the context of the HP14−cHP duplex, f_a from this substrate was reduced by half relative to that of C14. Since the proximal sequence of the labeled strand was identical for HP14, C14, and the HP14−cHP duplex, nearest neighbor effects cannot explain the composite of these results; rather, the decrease in f_a values for 2-AP specifically in the HP14−cHP duplex context can be attributed to extensive shielding resulting from base pairing with the complementary strand, analogous to decreases in f_a values for stem-positioned 2-AP (HP21 and HP21s) or its cognate duplex (HP21−cHP) relative to an unstructured control (C21).

Beyond the examples presented in this work, recent literature has also demonstrated a need for more complex

models for analyzing 2-AP quenching data. Single-population Stern−Volmer analysis (eq 1) ignored significant curvature observed in the acrylamide quenching of a 2-AP-labeled loop motif from 16S rRNA (*33*). Aminoglycoside binding to this motif enhanced upward curvature in classical Stern−Volmer plots which was attributed to system heterogeneity. However, the high quenching sensitivity ($K_{SV} > 18\ M^{-1}$) even in the absence of the drug suggests that a sphere of action model (eq 3) may be more appropriate. Conversely, addition of the drug neamine induced pronounced downward curvature in these plots, from which fractional accessibility assessments could have provided indices of conformational partitioning or local base pair dynamics. A second study (*27*) used fluorescence quenching experiments to distinguish contradicting structural models for a DNA quadruplex. Significant differences were seen in quenching curvature as a function of labeling position, but no quantitative analysis was described. Application of bimodal or sphere of action models to these and similar studies would allow more quantitative interpretation of quenching data, providing novel insights into the heterogeneity and/or local conformational dynamics of nucleic acid models.

Assessment of RNA Structure and Dynamics through Complementary Studies of Quenching and Fluorescence Intensity Measurements. The use of 2-AP fluorescence quenching to monitor local structural dynamics in nucleic acids potentially circumvents two factors which often conspire to confound spectroscopic studies. First, the sensitivity of 2-AP fluorescence to only its local environment reduces or eliminates the complications of globally merged signals measured by spectroscopic methodologies such as circular dichroism, UV/vis/IR spectroscopy, etc. (*4*). A second concern is that a given technique must detect processes occurring on a time scale appropriate for the question of interest. For example, while the quantum yield changes seen in our previous study successfully monitored RNA hairpin helix−coil transitions from diverse structural perspectives, they gave no indication of the localized duplex breathing suggested by nuclease digestion experiments (*4*). In contrast, fluorescence quenching provided multiple lines of evidence that the stem-positioned 2-AP experiences rapid base pair dynamics (see Results), using a method that is minimally demanding of time and resources.

Our current and previous studies illustrate that the most effective means of observing localized structural phenomena or conformational dynamics depend on the nature of event itself. Nucleotide stacking resulting from base pair interactions (e.g., HP21) was best observed using collisional quenching of 2-AP fluorescence, based on the substantial decrease in fractional solvent accessibility relative to unstructured control substrates. Conversely, fluorescence intensity changes successfully detected helix−coil transitions of the hairpin loop position [HP14 (*4*)], whereas acrylamide quenching could not distinguish the folded and unfolded states from this perspective. Helix−coil transitions exhibit differing fluorescence signatures and sensitivities depending on the nature of the associated RNA secondary structures. Finally, localized breathing dynamics within the hairpin stem region were best visualized using fluorescence quenching experiments. These findings indicate that concerted application of both fluorescence quantum yield and quencher sensitivity studies can provide a more comprehensive assessment of RNA conformational and dynamic events from diverse perspectives than by either approach in isolation. Furthermore, these methodologies are generally easy to implement, require relatively inexpensive equipment, and provide detailed, quantitative information describing local RNA mobility and thermodynamics that cannot be conveniently obtained by other techniques. Together, these orthogonal fluorescence approaches utilize the local sensitivity of 2-AP fluorescence to provide a powerful toolset which can aid in the de novo characterization of nucleic acid structure and conformational dynamics.

REFERENCES

1. Ward, D. C., Reich, E., and Stryer, L. (1969) Fluorescence studies of nucleotides and polynucleotides. I. Formycin, 2-aminopurine riboside, 2,6-diaminopurine riboside, and their derivatives. *J. Biol. Chem. 244*, 1228–1237.
2. Rist, M. J., and Marino, J. P. (2002) Fluorescent nucleotide base analogs as probes of nucleic acid structure, dynamics and interactions. *Curr. Org. Chem. 6*, 775–793.
3. Millar, D. P. (1996) Fluorescence studies of DNA and RNA structure and dynamics. *Curr. Opin. Struct. Biol. 6*, 322–326.
4. Ballin, J. D., Bharill, S., Fialcowitz-White, E. J., Gryczynski, I., Gryczynski, Z., and Wilson, G. M. (2007) Site-specific variations in RNA folding thermodynamics visualized by 2-aminopurine fluorescence. *Biochemistry 46*, 13948–13960.
5. Lee, B. J., Barch, M., Castner, E. W., Volker, J., and Breslauer, K. J. (2007) Structure and Dynamics in DNA Looped Domains: CAG Triplet Repeat Sequence Dynamics Probed by 2-Aminopurine Fluorescence. *Biochemistry 46*, 10756–10766.
6. Davis, S. P., Matsumura, M., Williams, A., and Nordlund, T. M. (2003) Position dependence of 2-aminopurine spectra in adenosine pentadeoxynucleotides. *J. Fluoresc. 13*, 249–259.
7. Jean, J. M., and Krueger, B. P. (2006) Structural fluctuations and excitation transfer between adenine and 2-aminopurine in single-stranded deoxytrinucleotides. *J. Phys. Chem. B 110*, 2899–2909.
8. O'Neill, M. A., and Barton, J. K. (2004) DNA-mediated charge transport requires conformational motion of the DNA bases: Elimination of charge transport in rigid glasses at 77 K. *J. Am. Chem. Soc. 126*, 13234–13235.
9. Rai, P., Cole, T. D., Thompson, E., Millar, D. P., and Linn, S. (2003) Steady-state and time-resolved fluorescence studies indicate an unusual conformation of 2-aminopurine within ATAT and TATA duplex DNA sequences. *Nucleic Acids Res. 31*, 2323–2332.
10. Somsen, O. J. G., Hoek, V. A., and Amerongen, V. H. (2005) Fluorescence quenching of 2-aminopurine in dinucleotides. *Chem. Phys. Lett. 402*, 61–65.
11. Xu, D. G., and Nordlund, T. M. (2000) Sequence dependence of energy transfer in DNA oligonucleotides. *Biophys. J. 78*, 1042–1058.
12. Rachofsky, E. L., Osman, R., and Ross, J. B. A. (2001) Probing structure and dynamics of DNA with 2-aminopurine: Effects of local environment on fluorescence. *Biochemistry 40*, 946–956.
13. Hardman, S. J. O., and Thompson, K. C. (2006) Influence of base stacking and hydrogen bonding on the fluorescence of 2-aminopurine and pyrrolocytosine in nucleic acids. *Biochemistry 45*, 9145–9155.
14. Lakowicz, J. R. (1999) *Principles of Fluorescence Spectroscopy*, Kluwer Academic/Plenum, New York.
15. van den Bremer, E. T. J., Keeble, A. H., Visser, A. J. W. G., van Hoek, A., Kleanthous, C., Heck, A. J. R., and Jiskoot, W. (2004) Ligand-induced changes in the conformational dynamics of a bacterial cytotoxic endonuclease. *Biochemistry 43*, 4347–4355.
16. Thuduppathy, G. R., Craig, J. W., Kholodenko, V., Schon, A., and Hill, R. B. (2006) Evidence that membrane insertion of the cytosolic domain of Bcl-xL is governed by an electrostatic mechanism. *J. Mol. Biol. 359*, 1045–1058.
17. Padrick, S. B., and Miranker, A. D. (2001) Islet amyloid polypeptide: Identification of long-range contacts and local order on the fibrillogenesis pathway. *J. Mol. Biol. 308*, 783–794.
18. Kumar, A., Tyagi, N. K., Goyal, P., Pandey, D., Siess, W., and Kinne, R. K. H. (2007) Sodium-independent low-affinity D-glucose transport by human sodium/D-glucose cotransporter 1: Critical role of tryptophan 561. *Biochemistry 46*, 2758–2766.

19. Gao, H., Wang, Y. N., Fan, Y. G., and Ma, J. B. (2006) Interactions of some modified mono- and bis-β-cyclodextrins with bovine serum albumin. *Bioorg. Med. Chem. 14*, 131–137.
20. Provitera, P., Bouamr, F., Murray, D., Carter, C., and Scarlata, S. (2000) Binding of equine infectious anemia virus matrix protein to membrane bilayers involves multiple interactions. *J. Mol. Biol. 296*, 887–898.
21. Gorbenko, G. P., Ioffe, V. M., and Kinnunen, P. K. J. (2007) Binding of lysozyme to phospholipid bilayers: Evidence for protein aggregation upon membrane association. *Biophys. J. 93*, 140–153.
22. Nandi, P. K., Bera, A., and Sizaret, P. Y. (2006) Osmolyte trimethylamine N-oxide converts recombinant α-helical prion protein to its soluble β-structured form at high temperature. *J. Mol. Biol. 362*, 810–820.
23. Brewer, B. Y., Ballin, J. D., Fialcowitz-White, E. J., Blackshear, P. J., and Wilson, G. M. (2006) Substrate dependence of conformational changes in the RNA-binding domain of tristetraprolin assessed by fluorescence spectroscopy of tryptophan mutants. *Biochemistry 45*, 13807–13817.
24. Yi-Brunozzi, H. Y., Stephens, O. M., and Beal, P. A. (2001) Conformational changes that occur during an RNA-editing adenosine deamination reaction. *J. Biol. Chem. 276*, 37827–37833.
25. Deb, S., Bandyopadhyay, S., and Roy, S. (2000) DNA sequence dependent and independent conformational changes in multipartite operator recognition by λ-repressor. *Biochemistry 39*, 3377–3383.
26. Sha, M., Wang, Y., Xiang, T., van Heerden, A., Browning, K. S., and Goss, D. J. (1995) Interaction of wheat germ protein synthesis initiation factor eIF-(iso)4F and its subunits p28 and p86 with m^7GTP and mRNA analogues. *J. Biol. Chem. 270*, 29904–29909.
27. Li, J., Correia, J. J., Wang, L., Trent, J. O., and Chaires, J. B. (2005) Not so crystal clear: The structure of the human telomere G-quadruplex in solution differs from that present in a crystal. *Nucleic Acids Res. 33*, 4649–4659.
28. Stivers, J. T. (1998) 2-Aminopurine fluorescence studies of base stacking interactions at abasic sites in DNA: Metal-ion and base sequence effects. *Nucleic Acids Res. 26*, 3837–3844.
29. Tleugabulova, D., and Reha-Krantz, L. J. (2007) Probing DNA polymerase-DNA interactions: Examining the template strand in exonuclease complexes using 2-aminopurine fluorescence and acrylamide quenching. *Biochemistry 46*, 6559–6569.
30. Malta, E., Moolenaar, G. F., and Goosen, N. (2006) Base flipping in nucleotide excision repair. *J. Biol. Chem. 281*, 2184–2194.
31. Walter, N. G., Harris, D. A., Pereira, M. J. B., and Rueda, D. (2001) In the fluorescent spotlight: Global and local conformational changes of small catalytic RNAs. *Biopolymers 61*, 224–242.
32. Sakamoto, T., Mahara, A., Yamagata, K., Iwase, R., Yamaoka, T., and Murakami, A. (2005) Evaluation of dynamic features of *Escherichia coli* 16S ribosomal RNA in homogeneous physiological solution. *Biophys. J. 89*, 4122–4128.
33. Chao, P. W., and Chow, C. S. (2007) Monitoring aminoglycoside-induced conformational changes in 16S rRNA through acrylamide quenching. *Bioorg. Med. Chem. 15*, 3825–3831.
34. Balbo, P. B., Toth, J., and Bohm, A. (2007) X-ray crystallographic and steady state fluorescence characterization of the protein dynamics of yeast polyadenylate polymerase. *J. Mol. Biol. 366*, 1401–1415.
35. Hermann, T., and Patel, D. J. (2000) RNA bulges as architectural and recognition motifs. *Structure 8*, R47–R54.
36. Borer, P. N., Lin, Y., Wang, S., Roggenbuck, M. W., Gott, J. M., Uhlenbeck, O. C., and Pelczer, I. (1995) Proton NMR and structural features of a 24-nucleotide RNA hairpin. *Biochemistry 34*, 6488–6503.
37. Ennifar, E., and Dumas, P. (2006) Polymorphism of bulged-out residues in HIV-1 RNA DIS kissing complex and structure comparison with solution studies. *J. Mol. Biol. 356*, 771–782.
38. Berglund, J. A., Rosbash, M., and Schultz, S. C. (2001) Crystal structure of a model branchpoint-U2 snRNA duplex containing bulged adenosines. *RNA 7*, 682–691.
39. Jaeger, J. A., and Tinoco, I. (1993) An NMR study of the HIV-1 TAR element hairpin. *Biochemistry 32*, 12522–12530.
40. Colvin, R. A., White, S. W., Garcia-Blanco, M. A., and Hoffman, D. W. (1993) Structural features of an RNA containing the CUGGGA loop of the human immunodeficiency virus type 1 transactivation response element. *Biochemistry 32*, 1105–1112.
41. Klinck, R., Sprules, T., and Gehring, K. (1997) Structural characterization of three RNA hexanucleotide loops from the internal ribosome entry site of polioviruses. *Nucleic Acids Res. 25*, 2129–2137.
42. Wilson, G. M., Sun, Y., Lu, H., and Brewer, G. (1999) Assembly of AUF1 oligomers on U-rich RNA targets by sequential dimer association. *J. Biol. Chem. 274*, 33374–33381.
43. Myers, R. H. (1990) Criteria for choice of best model. In *Classical and Modern Regression with Applications*, 2nd ed., pp 164−208, PWS-KENT Publishing Co., Boston.
44. Madan, B., and Sharp, K. A. (2001) Hydration heat capacity of nucleic acid constituents determined from the Random Network Model. *Biophys. J. 81*, 1881–1887.
45. Poland, D., Vournakis, J. N., and Scheraga, H. A. (1966) Cooperative interactions in single-strand oligomers of adenylic acid. *Biopolymers 4*, 223–235.
46. Bloomfield, V. A., Crothers, D. M., and Tinoco, I., Jr. (2000) *Nucleic Acids: Structure, Properties and Functions*, University Science, Sausalito, CA.
47. Dornberger, U., Hillisch, A., Gollmick, F. A., Fritzsche, H., and Diekmann, S. (1999) Solution structure of a five-adenine bulge loop within a DNA duplex. *Biochemistry 38*, 12860–12868.
48. Smoluchowski, M. V. (1917) Versuch einer mathematischen theorie der koagulationskinetik kolloider lösungen. *Z. Phys. Chem. 92*, 129–168.
49. Eftink, M. R., and Ghiron, C. A. (1976) Fluorescence quenching of indole and model micelle systems. *J. Phys. Chem. 80*, 486–493.
50. Kawahara, K., and Tanford, C. (1966) Viscosity and density of aqueous solutions of urea and guanidine hydrochloride. *J. Biol. Chem. 241*, 3228–3232.

BI800487C